Imaging a shallow salt diapir using ambient seismic vibrations beneath the densely built-up city area of Hamburg, Northern Germany

Article *in* Journal of Seismology · July 2011

DOI: 10.1007/s10950-011-9234-y

CITATIONS
19

READS
282

3 authors, including:

Matthias Ohrnberger
Universität Potsdam
154 PUBLICATIONS **4,876** CITATIONS

SEE PROFILE

Torsten Dahm
Helmholtz-Zentrum Potsdam - Deutsches GeoForschungsZentrum GFZ
322 PUBLICATIONS **6,099** CITATIONS

SEE PROFILE

Journal of Seismology manuscript No.
(will be inserted by the editor)

Imaging a shallow salt diapir using ambient seismic vibrations beneath the densely built-up city area of Hamburg, Northern Germany

D. Kühn · M. Ohrnberger · T. Dahm

Received: date / Accepted: date

Abstract Salt diapirs are common features of sedimentary basins. If close to the surface, they can bear a significant hazard due to possible dissolution sinkholes, karst formation and collapse dolines or their influence on ground water chemistry. We investigate the potential of ambient vibration techniques to map the 3-D roof morphology of shallow salt diapirs.

H/V spectral peaks are derived at more than 900 positions above a shallow diapir beneath the city area of Hamburg, Germany, and are used to infer the depth of the first strong impedance contrast. In addition, 15 small-scale array measurements are conducted at different positions in order to compute frequency-dependent phase velocities of Rayleigh waves between 0.5 and 25 Hz. The dispersion curves are inverted together with the H/V peak frequency to obtain shear wave velocity profiles.

Additionally, we compare the morphology derived from H/V and array measurements to borehole lithology and a gravity-based 3-D model of the salt diapir. Both methods give consistent results in agreement with major features indicated by the independent data. An important result is that H/V and array measurements are better suited to identify weathered gypsum caprocks or gypsum floaters, while gravity-derived models better sample the interface between sediments and homogeneous salt. We further investigate qual-

D. Kühn

NORSAR, P. O. Box 53, 2007 Kjeller, Norway

Tel.: +47-63805-933

Fax: +47-6381-8719

E-mail: daniela@norsar.no

M Ohrnberger

Department of Geosciences, University of Potsdam, Karl-Liebknecht-Strasse 24, Haus 27, 14476 Potsdam, Germany

T. Dahm

Institute of Geophysics, University of Hamburg, Bundesstr. 55, 20146 Hamburg, Germany

itatively the influence of the 3-D subsurface topography of the salt diapir on the validity of local 1-D inversion results from ambient vibration dispersion curve inversion.

Keywords ambient seismic vibrations · H/V method · array measurements · salt diapir · 3-D effects

1 Introduction

The deeper underground of the metropolitan region of Hamburg, Northern Germany, is geologically characterised by poorly consolidated sediments at shallow depths and emplacement of salt diapirs (Ehlers, 1995; Reinhold et al, 2008; Dahm et al, 2010b). In such a heavily built-up urban region with its high concentration of buildings, industrial plants, and traffic routes, potential geohazards have to be explored. Especially close to the surface, the risk of local dissolution of evaporitic rocks by ground water is high. Subrosion and karst may lead to subsidence, the formation of instable cavities and finally to the development of sinkholes and solution dolines. During the 20th century, 20 collapse microearthquakes took place and so far, more than 30 sinkholes and dolines are known in the metropolitan region (Dahm et al, 2010a).

We gathered information on the most prominent salt diapir (Othmarschen-Langenfelde diapir). Since the use of active seismic exploration techniques is prohibitive in large parts of the urban environment, we explored the possibilities of using passive recordings of urban seismic noise to map the depth of the salt dome interface which represents a strong impedance contrast in shear wave velocity. In recent years, ambient seismic vibration has emerged as a valuable tool to obtain subsurface shear wave velocity profiles, especially in regions covered by soft sediments. Advantages of the method are its low costs, the non-destructivity of measurements and such its applicability even in densely populated areas, see e.g. for microzonation studies (Panou et al, 2005, Thessaloniki), (Cara et al, 2008, Palermo) or (Birgören et al, 2009, Istanbul) as well as Asten and Henstridge (1984), Matsushima and Okada (1990), Yamanaka et al (1994), Tokimatsu (1997), Kawase et al (1998), Satoh et al (2001), and Scherbaum et al (2003) for estimation of shear wave velocity structure. Whereas the presence of strong seismic noise, regardless of its origin (i.e. anthropogenic activities like traffic or industry or natural sources like microseisms), is obstructive for active seismic investigations, it represents a continuous energy source for passive seismic measurements illuminating the subsurface. A set of useful guidelines were developed within the framework of the EU-project SESAME (Site effects assessment using ambient excitations, see e.g. SESAME group, 2005; Jongmans et al, 2005).

Single station as well as small aperture array recordings were performed. For the single station measurements, H/V ratios are investigated. Rayleigh wave dispersion curves determined from array measurements are inverted together with

the H/V peak frequency to derive the shear wave velocity profile at the measurement site. For the estimation of high quality dispersion curves, it is important to capture the wave field properties in the broadest possible frequency range. Because of the limited number of sensors, a repeated deployment of stations is necessary. To simplify repetitions of station deployments especially in urban environments, we used a wireless array analysis system (WARAN) developed by the Department of Geosciences, University of Potsdam, facilitating real time array analysis during the ongoing field measurement. This approach allows exploring the resolution limits of the array measurement and adjusting the geometry of subsequent array setups to the particularly observed wave field situation.

Prior information on density as well as compressional and shear wave velocities at shallow depth can be used to reduce the non-uniqueness during inversion. Therefore, a gravimetric survey on 500 landmark points has been performed and shallow hammer blow refraction seismic surveys complement the array measurements where possible. Details on the inversion of the micro-gravimetric survey as well as an extensive compilation of existing knowledge and data for evaluation of sinkhole and karst formation can be found in Dahm et al (2010b). They compare the salt model to yearly subsidence rates, surface deformation, temperature and hydraulic head in aquifers as well as chemical analyses of the ground water. The results indicate an ongoing dissolution process that may affect the urban development.

1.1 Ambient seismic vibrations

It has been widely demonstrated (Aki, 1957; Horike, 1985; Tokimatsu, 1997; Okada, 2003) that the analysis of ambient vibration wave fields is a valuable tool for characterising the shallow subsurface characteristics in terms of shear wave velocity structure. The energetically dominating parts of seismic ambient vibration wave fields consist mainly of surface waves. In particular Rayleigh waves show two properties which can be used to derive physical properties of the subsurface: the frequency-dependent ellipticity of motion and the frequency-dependent propagation velocity (dispersion). Both characteristics can be related to 1-D depth profiles of shear wave velocity. Two distinct types of measurements were used to map the extent and depth of the Othmarschen-Langenfelde salt diapir, single station 3-component recordings for the determination of H/V ratios, and small aperture seismic array recordings for the determination of the dispersion curve. Peak frequencies and dispersion curves are used in combination to invert for the best fitting shear wave velocity profile at the measurement site.

Small-scale seismological arrays can be used to estimate the frequency-dependent phase-velocity of short-wavelength Rayleigh waves propagating in uppermost soil and sediments. This is either accomplished with active experiments employ-

ing point sources or by analysing the statistical properties of the frequency-wavenumber spectra of ambient noise. The use of Rayleigh wave dispersion curves for determining shear wave velocity profiles is well established in ambient vibration studies (Horike, 1985; Ishida et al, 1998; Miyakoshi et al, 1998; Yamamoto, 1998). Although logistically demanding, array techniques allow the direct estimation of wave propagation characteristics, i.e. apparent wave velocity and direction of the impinging seismic wave front. Frequency-wavenumber (f-k, e.g. Capon, 1969; Tokimatsu, 1997) and auto-correlation techniques (Aki, 1957) are widely used to obtain the apparent phase velocities in narrow frequency bands. The resulting frequency-dependent phase velocities are interpreted in terms of dispersion branches of surface waves which permit to invert for the physical quantities of 1-D earth models parameterised as stack of layers. Constituting a highly non-linear and non-unique inverse problem, it is of crucial importance to obtain an accurate dispersion curve over a wide frequency band and a well-founded interpretation of observations in the first place. Thus, considering the narrow band resolution capabilities of array settings with only a few sensors, adaptive layout strategies have been proposed to capture the full available wavelength range of the surface waves present in ambient vibration wave fields (Asten and Henstridge, 1984; Ohrnberger et al, 2004a,b, 2005). Further, accompanying geophysical measurements (shallow hammer blow refraction seismic, gravimetry) may add valuable a priori information for the reduction of non-uniqueness of the inverse problem.

The single station H/V analysis techniques (Nogoshi and Igarashi, 1971; Nakamura, 1989; Bard, 1999) allow the estimation of the fundamental resonance period of low impedance sediment layers overlaying much higher impedance materials (bedrock or in our case salt). The physical interpretation of this fundamental period is still ambiguous, both reverberating SH body waves, the Airy phase of Love waves as well as the ellipticity characteristics of Rayleigh surface waves may account for the observation of a peak in the H/V spectral ratios. However, it has been shown that for large impedance contrasts in simple structures both hypotheses may explain the observation equally well as response of the subsurface to the seismic excitation (Malischewsky and Scherbaum, 2004). Whereas especially the H/V method was originally developed to perform microzonation surveys for earthquake hazard (Mooney and Bolt, 1966; Lachet and Bard, 1994; Tokimatsu, 1997), it emerged later on as geophysical exploration tool to assess soil and sedimentary thickness, ranging from tens of metres to more than 1000 m (Ibs von Seht and Wohlenberg, 1999; Delgado et al, 2000; Parolai et al, 2002). Partly, the H/V spectrum has even been used to obtain shear wave velocity profiles (Arai and Tokimatsu, 1998; Ishida et al, 1998; Miyakoshi et al, 1998; Fäh et al, 2001; Arai and Tokimatsu, 2004) based on the interpretation of being the

fundamental mode Rayleigh wave ellipticity response of the underlying subsurface structure.

Both, the H/V model and the depth of the dominant impedance contrast estimated from Rayleigh wave dispersion are non-unique. Often, a trade-off between accumulated travel-times in the sediment structure and the depth of the main impedance contrast is observed. This suggests the usage of combined inversion strategies from H/V information and dispersion information obtained from array measurements (Scherbaum et al, 2003; Parolai et al, 2005; Picozzi et al, 2005).

1.2 The Othmarschen-Langenfelde diapir

From all the salt diapirs situated in the subsurface of Hamburg, Northern Germany (Fig. 1, left), only the Othmarschen-Langenfelde diapir, abbreviated by OLD in the following, reaches almost to the surface, whereas the others are stuck at larger depths. Its existence as well as the presence of a karst system has been known for some time; the residual gypsum caprock has been exploited in the past and the karst system was recognised in connection with collapse earthquakes and the formation of sinkholes. Sinkhole features and historical collapse earthquakes in the southern (more shallow) part of the OLD have been mapped by e.g. Niedermayer (1962), Grube (1973) and Paluska (2002). Sinkholes within the metropolitan area can be as large as 100 m in diameter (Bahrenfelder See) and may have depth extensions of up to 185 m (Grube, 1973).

In spite of its importance for the urban development due to the associated hazard, the OLD has not yet been studied in detail. Especially the distribution and extent of possible gypsum karst and its related hazard is not known, although the repeated occurrence of collapse earthquakes at partly identical positions suggests a widely spread presence of gypsum karst beneath at least the southern part of the OLD. It is unclear if the karst system evolved during paleoperiods or if its formation is an ongoing process. An additional hazard is posed due to potential anthropogenic influence on salt dissolution. Man-induced formation of sinkholes or collapse earthquakes is well known from other urban areas in gypsum karst regions (Benito et al, 1995; Soriano and Simon, 1995, 2002; Waltham et al, 2005; Johnson, 2008).

The metropolitan region of Hamburg is home to 2 million inhabitants and is located in a late tertiary basin. The OLD is part of the so-called ”salt giant” of several hundred metres thickness being situated within the 10-12 km thick sediments of the North German basin at a depth of 4.5 km. This salt giant developed during the Late Permian to the late Triassic when the northern European basin was covered by the shallow epicontinental Zechstein Sea (Scheck-Wenderoth et al, 2008). Halokinese (vertical flow of salt) triggered in Triassic resulted in diapirs situated along the strike direction of deeper faults (Geluk et al, 2007; Scheck-Wenderoth et al, 2008). The OLD halokinese was triggered in Cretaceous-Tertiary (Scheck-Wenderoth et al, 2008; Jaritz,

1987; Warren, 2006) and is nowadays characterised by salt walls elongated in N-NE direction having steep flanks at the eastern and western border. At depth, the OLD is possibly connected to a broader and larger salt pillow. The OLD has an along strike dimension of approximately 20 km. Its southern border seems to coincide with the Elbe lineament which represents a deep rooted system, but it is not clear if the OLD diapir is controlled by it (Ehlers, 1995).

Gripp (1920) gathered information on caprocks and residual gypsum at diapirs in North Germany and concluded that the OLD may currently undergo subsidence due to subrosion and salt dissolution. These findings are supported by measurements of relative uplift (1.2 mm/y) and subsidence (3.5 mm/y) during 1960-1970 (Fleischhauer, 1979). Niedermayer (1962) analysed borehole stratigraphies in the southern part of the OLD. Both Gripp (1920) and Niedermayer (1962) tried to map depth and thickness of the residual gypsum layer as well as locations of subsidence depressions, sinkholes, and void space found in drill cores at deeper levels and interpreted as evidence of gypsum karst. Plaumann (1979) developed a geometrical model of the diapir based on gravity data and found a bowl-shaped roof. Prexl (1997) analysed high resolution seismic data to study the roof morphology and found different geometrical shapes at the eastern and western borders as well as a southward extension of the OLD beneath the Elbe River.

2 Description of measurements

Between January 2006 and August 2007, 303 single station as well as 15 array measurements (comprising 660 station positions) have been performed using Lennartz 5-s three-component sensors. For array measurements, 8 sensors were usually available. Single station and array measurement sites (as individual stations) are visible in Fig. 1 (right). The city area of Hamburg and its districts are displayed in light grey. The salt dome outline is plotted in red as given by Grube (1973). Single station measurement sites are depicted by green, array station measurement sites by blue points. A grid with 1 km spacing underlies the single station positions. At points of interest, mainly in the South where the salt dome lies near to the surface, the grid has been refined to distances of only a few tens of metres. Further, the spacing is minimised at array measurement sites since individual array stations can be treated as single stations. Both single station analysis and array analysis are performed using the *geopsy* software package[1] (Wathelet, 2005). Additionally, borehole stratigraphies were made available by the Geological Survey of Hamburg, their positions are marked by red points.

[1] available at www.geopsy.org

2.1 Array measurements

2.1.1 The wireless array measurement and analysis system

The estimation of high quality dispersion curves requires to capture the wave field properties in the broadest possible frequency range (Ohrnberger et al, 2005). Since the spatial sampling of the wave field is sparse and a trade-off exists between array geometry and the range of analysable wavelengths and further, the spectral content of the wave field and propagation velocities are not known a priori, a repeated deployment of array geometries is suggested. A new generation of hard- and software tools has been developed in order to obtain analysis results immediately during the field experiment, enabling not only a direct comparison of the resolution/aliasing limits of the ongoing array measurement but also allowing for a build-up of prior information, thus providing a basis to react on particular wave field situations and to adjust measurement geometries.

In order to accomplish the real time in-field data acquisition and transmission to a central field computing facility (laptop), we attached specialised embedded Linux devices with wireless connectivity to AD-converters. The key element of this custom system is the use of open source wireless LAN networking protocols, called mesh protocols (Tønnesen, 2004). The mesh protocol enables the devices to automatically organise themselves within short time (typically less than a minute) as a multipoint-to-multipoint wireless LAN in a MANET (mobile ad-hoc network) topology. Fig. 2a shows one example for such a self-organised network. The measurement starts with a small scale array with an aperture of about ten metres, and the aperture is subsequently increased after 20 to 40 minutes of measurements. Data acquisition takes place at each individual sensor position and the same acquisition nodes self-organise to build the MANET topology on the fly after each re-arrangement. The digitized waveform data is stored locally (for redundancy) but also immediately transmitted within the MANET to the central processing unit, i.e. a standard laptop. For ensuring a full mesh-coverage and enabling all sensors to be reached by the central field processing unit, additional repeater nodes (green circles in Fig. 2, left) can be used to allow for an extension of the achievable array dimension in logistically difficult environments. Fig. 2 (right) shows an example record of ambient noise of 40 minutes length. Data are already processed and analysed in the field during the measurement, and array configuration and measurement duration could interactively be optimised during each deployment.

The real time data analysis tools have been implemented as software clients attaching to a seedlink server (Hanka et al, 2000) accessing the real time data feeds at the central field computing facility and providing means for buffering the data in both memory and file buffers. The advantage of this equipment is many-fold:

- The direct control of full array waveforms enables to immediately detect unfavourable noise conditions, installation deficiencies or equipment failure.
- The in-field processing of waveform data allows determining when sufficient data has been acquired and when to proceed to the next array configuration for continuing the measurement without delays.
- No static routing tables have to be used, all systems operate equally as sender, receiver, or repeater. Routing tables are created on the fly and are shared among the operating acquisition nodes. Any device can be reached from any other (including the central collecting and processing device) in few network hops.
- Since the equipment is easy to deploy in normally difficult environments for wireless transmission (e.g. urban areas), the time required for installation is reduced substantially.
- The equipment is light weight and has a low power consumption.

The waveforms acquired in real time at the central field processing unit are instantaneously visualised and analysed. The array analysis software is derived from freely available GPL licensed source code for continuous array processing of ambient vibration recordings developed in the SESAME project (CAP, *Continuous Array Processing*; Ohrnberger et al, 2004a,b, 2005) as well as libslink by Chad Trabant.

2.1.2 Description of specific arrays

In total, 15 sites above the diapir have been used for array measurements. At every site, several arrays (3-8) with different apertures have been deployed. Arrays with small aperture typically were built up as circle including a centre station to sensibilise the arrays for noise from all directions. For larger arrays, the circular configuration mostly could not be maintained due to limitations resulting from building density and infrastructure. An overview on array sizes and numbers of arrays measured at each site can be found in Table 1. Due to the large heterogeneity visible already in the H/V spectra, the site Jenischpark was split into two sites (JEN1 and JEN2) for further analysis. At eight sites situated in parks (marked by *), hammer blow refraction seismic have been performed to receive an impression of P- and S-wave velocities within the upper layers of the subsurface. S-waves were excited by blowing the hammer on a steel plate buried halfway in line with the seismic profile. The deepest refraction recorded resulted from an interface at 50 m depth. In most cases, a very shallow interface (most probably ground water) was found at depths of 2-5 m. P-wave velocities in the uppermost layer ranged from 300 m/s to 550 m/s, and in the subsequent layer from 1000 m/s to 1800 m/s. S-wave velocities were almost exclusively measured in the uppermost layer and ranged from 130 m/s to 350 m/s.

Table 1 Numbers and apertures of arrays; as aperture of the array, the largest distance between any two stations is indicated;* marks the sites where a hammer blow refraction seismic survey has been performed in addition

site name	abbreviation	no of arrays	min. aperture (m)	max. aperture (m)
Altonaer Volkspark*	AVP	4	10	124
Borehole North	BOHR1	7	21	1098
Borehole South*	BOHR2	7	6	321
Cranachplatz*	CRAN	4	12	417
Kolonie am Diebsteich	DIEB	4	11	157
Gloxinienweg	GLOX	5	20	295
Sportplatz Heidlohstr	HEID	6	13	336
Holloswisch*	HOLLO	7	12	831
Jenischpark East	JEN1	4	12	259
Jenischpark West*	JEN2	4	13	646
Wassermannpark*	KK	7	12	651
Kleingartenverein 308	KLGV308	3	15	298
Niewisch*	NIE	7	11	679
Pfitzner Str*	PFS06	3	18	212
Sprützwiese	SPRUETZ	6	8	570
Wiebelstr	WIEBEL	6	7	457

2.2 Single station measurements

For analysis of the single station measurements, the H/V method, also known as Nakamura's technique, is used. It was first introduced by Nogoshi and Igarashi (1971) and refined by Nakamura (1989). The horizontal-to-vertical (H/V) spectral ratio of micro-tremors, observed at a site using a three-component sensor, may yield information on impedance contrasts in the subsurface. Time traces, having a typical length of 30-45 min, were checked for monochromatic, man-made signals (random decrement technique; see Michel et al, 2008, for details; we employed it as implemented in the *geopsy damping toolbox)* and if the check was negative, they were subdivided into time windows of 60 s. Each time window was detrended, tapered with a 10% cosine taper and Fourier transformed. Spectra were smoothed by the Konno and Ohmachi (1998) algorithm using a b-value of 40. Subsequently, the East and North component spectra were combined by the geometrical mean and both ratios between East and vertical component spectra, North and vertical component spectra, and combined horizontal and vertical compo-

nent spectra are computed. The combined spectra will be used for further analysis. The final H/V ratio was obtained by averaging the H/V ratios from all time windows using again the geometrical mean. If a strong impedance contrast exists in the subsurface, a spectral peak can be found (see e.g. Fäh et al, 2001, for the theoretical background). The peak frequency depends on the depth of the impedance contrast and the overlying average velocities of the sediment layers. A peak at low frequencies is caused by a deeper impedance contrast than a peak at higher frequencies (assuming similar wave propagation characteristics within the sediment coverage at both sites). Some authors regard the presence of multiple peaks as indication for the presence of multiple impedance contrasts at different depths (see e.g. Picozzi et al, 2009). However, we disregarded the presence of multiple peaks and used only the lowest-frequency peak. In Fig. 3, H/V spectra measured outside the salt diapir (left) and above the salt diapir (right) are depicted exemplarily. Spectra from different time windows are distinguished by their grey scale, the vertical grey bars give the standard deviation of the automatically identified H/V peak frequency. In the H/V spectra at the left, no specific features can be identified. In the H/V spectra on the right, measured above the salt diapir, a clear peak is observed at 1.1 Hz. The variation of spectra between different time windows is higher than on the left, reflecting the higher irregularity of the noise source.

Table 2 Typical geophysical parameters for rock types relevant to this study; * after Zimmer (2001), ** from own measurements (hammer blow refraction seismic), *** after Rumpel et al (2005),**** after Wiederhold et al (2002)

rock type	v_P (m/s)	v_S (m/s)	ρ (kg/m^3)
sand, sandstone**	300-1800	130-350	–
sand, sandstone	500-2150***	150-600***	2000-2100****
clay	1700-1800***	370-400***	1800-1980****
gypsum*	4750 5800	2500	2250-2310
anhydrite*	5700-6100	3300	2800 - 2930
rock salt*	3600-4700	2300-2600	2170

3 Diapir interface

3.1 Borehole stratigraphies

Shallow stratigraphic layers in the Hamburg metropolitan area mainly consist of sediments, either loose sand, sandstone, silt, or clay. Some typical geophysical parameters for those rock types including rock salt, anhydrite and gypsum are collected in Table 2. For sand and clay, we will use values measured north of Hamburg (Rumpel et al, 2005) including our own hammer blow refraction seismic. For gypsum, anhydrite and rock salt, we will employ values measured in salt mines in Northern Germany (Zimmer, 2001). Most of the boreholes conducted over the years [2] are shallow since they have been drilled for exploitation of fresh water, for quality control of ground water or as pre-site surveys for larger construction sites. However, several boreholes reach

[2] source: Geological Survey of Hamburg

the caprock and show gypsum (often layered or mingled with clay or sandstone). A selection is shown in Fig. 4 sorted by latitude, the southernmost profile is shown to the left, the northernmost to the right. In general, the caprock is reached at shallower depths in the South of the city area. Only two boreholes reach down into the salt diapir itself revealing rock salt at depths of 203 and 457 m, respectively (in borehole 6036-C2, the rock salt is mingled with gypsum down to a depth of 414 m, whereas in borehole 6044-C18 it is overlaid by anhydrite). In one single borehole, a more than 500 m thick layer of limestone and chalk is declared (borehole 6246-C13) overlaying a gypsum layer at a depth of 1401 m. Since it is much deeper than the other boreholes, it is not shown here.

3.2 Diapir interface depth derived from H/V method

To convert H/V peak frequencies into depth of the impedance contrast, a relation of the type

$$h = a \cdot f^b \quad (1)$$

can be used where h is the depth of the impedance contrast, f is the peak frequency and a and b are parameters (Ibs von Seht and Wohlenberg, 1999). This formula represents a velocity-depth function for the sediment block above the first impedance contrast and is therefore independent of the underlying material. The parameters a and b depend on the local geology, especially the shear wave velocity, and were given for German sites e.g. by Ibs von Seht and Wohlenberg (1999) for the Western Lower Rhine Embayment (a=96, b=-1.388), by Hinzen et al (2003) for the Lower Rhine Embayment (a=108, b=-1.551) and by Parolai et al (2002) for the Cologne area (a=137, b=-1.190). Due to this variation, we derived an own set of parameters using borehole stratigraphies, H/V peak frequencies and array measurements (see Fig. 5). We compared H/V spectra measured at borehole sites to spectra computed from the borehole stratigraphies to identify the layer causing the peak in the frequency spectrum (either gypsum, salt or clay) and used its depth together with the measured peak frequency for the regression (displayed in Fig. 5 by grey diamonds). Not at all borehole sites, measurements were successful. Therefore, only the depth range between 52 m and 133 m could be covered, and these depth-frequency pairs were combined for regression with pairs found from dispersion curve inversion (shown by black diamonds), using the H/V peak frequency employed in the inversion and the depth of the impedance contrast found from inversion (more information on the inversion of dispersion curves will be given in Section 3.3). Thus, the depth range could be expanded up to 585 m. A further constraint at greater depth could be gained from a gravity-based salt model (Dahm et al, 2010b). Error bars for H/V peak frequencies were deduced directly from the H/V curves. Error bars for the depth of the impedance contrast were derived from the shear wave velocity profiles resulting

from dispersion curve inversion (see Section 3.3) by computing the standard deviation for the best fitting 100 dispersion curves. We did not assume an error for interface depths read from the borehole profiles, since layer depths are given with an accuracy of about 1-2 m which is much smaller than the depths errors computed from shear wave profiles.

The nonlinear regression employing a least-squares algorithm is performed in logarithmic space and results in values for parameters a and b of a=125.29$\pm$13.91 and b=-1.07$\pm$0.15. The result is displayed by the black line in Fig. 5. The regression process is equivalent to averaging the depth dependency of the shear wave velocity over the salt diapir area. This now enables us to compute an interface depth out of the measured H/V peak frequencies (see Fig. 6). On the left, measured peak frequencies are shown with noticeable accumulation of points at array sites and within the refined grid areas in the South. H/V peak frequencies cover a range from 0.15 Hz (slightly beneath the eigenfrequency of the 5-s seismometers) to 2.72 Hz with the highest values situated in the South of the city area. In the middle, peak frequencies are converted into pseudo depths and on the right, pseudo depths are gridded using the GMT-tool *nearneighbor* (Wessel and Smith, 1991) to gain an impression of the interface appearance. Most likely, the interface is reflecting the caprock interface (see discussion in Section 4.2) and not the salt dome being situated considerably deeper. The caprock is very shallow in the South of the city area and gradually descends to the North. To the East, an elevated rim is visible. Within this rim, there seems to be a depression to the East of the salt dome, however, this observation is only based on a single point. A second depression is visible more to the North and is consistent with the presence of a Quaternary channel, the Ellerbeker Rinne, whose 400 m depth contour is marked by thin grey lines. Since the Ellerbeker Rinne cuts the Miocene Hamburg Clay which acts as a hydraulic barrier between the Miocene aquifers of the Upper and Lower Braunkohlensande (Gabriel et al, 2003), this depression may be caused by a dissolution process.

In addition, the locations of recent sinkholes (Buurman, 2009) are plotted on top by thin black lines forming polygons. They clearly agree with the western caprock high which is not surprising since gypsum karst is a common feature observed when gypsum layers reach close to the surface (Waltham et al, 2005; Warren, 2006).

The results also suggest that the diapir may extend further to the East than presently assumed.

3.3 Diapir interface depth derived from array measurements

Dispersion curves were determined from the ambient noise array recordings using the high-resolution f-k analysis routine as implemented in the *geopsy* software package (Wathelet, 2005). The underlying method was developed by Capon (1969) and is based on the picking of energy maxima in the wavenum-

ber plane for sliding time windows and narrow frequency bands. The method provides azimuth and slowness for the most coherent plane wave arrivals. The wavenumber grid search is performed using an iteratively refined grid-adjustment in order to allow for the accurate estimation of local maxima. The central frequencies of the frequency bands were sampled equidistantly on a logarithmic scale and the frequency bandwidth was defined to be 6% of the corresponding centre frequencies. The time window length was chosen as 200 times the central period. Usually, dispersion curves are extracted for each of the sub-arrays taking into account the resolution limits arising from the array geometry and joining the individual dispersion curves in one. In this study, we gathered the energy maxima for all array sizes into one single histogram and picked the resulting dispersion curve, minimum and maximum wave number limits for each sub-array being determined from their theoretical array response. Wathelet (2005) recommends to use dispersion curves only between k_{min} (resolution limit of the array) and $k_{max}/2$ (k_{max} being the aliasing limit of the array).

For inversion of the dispersion curves, the *geopsy*-tool *dinver* has been used. The inversion is performed using a neighbourhood algorithm (Sambridge, 1999a,b). The neighbourhood algorithm is based on subdividing the solution space into Voronoi cells and refining the sampling in regions of low misfit during each iteration. The misfit is defined by the distance between the calculated and experimental dispersion curve computed at every frequency sampling point. When various modes are identified, the inversion of all modes is performed employing a multi-modal misfit (for details, see Wathelet, 2005). Its implementation into the *dinver* software package is described by Wathelet et al (2004) and Wathelet (2008) and results in an ensemble of models explaining the data. The parameter range for P- and S-wave velocities at the surface is limited to values taken from hammer blow refraction seismic. As proposed by Fäh et al (2001, 2003) and Scherbaum et al (2003), a representative H/V peak frequency from the array stations (in most cases from the central station) is used as additional constraint, since the inversion of dispersion curves constrains mainly the velocity-depth relation whereas the ellipticity constrains mainly the layer thickness (for details on the implementation of both constraints and their influences on the misfit see Wathelet, 2005).

For half of the array sites, only a fundamental mode dispersion curve could be found. At a third of the sites, a fundamental mode as well as a higher mode dispersion curve could be identified and at sites BOHR1 and JEN, we recognised the fundamental mode dispersion curve and two higher modes. As basic model, a layer over half-space model is chosen consistent with the analysis of the H/V peak frequencies. The upper layer is subdivided into ten sub-layers and compressional and shear wave velocity are allowed to increase either linearly or by power law. Only sites AVP,

BOHR1 and PFS06 can be fitted better using a linear increase of velocity, all other sites can be adapted better using a power law velocity increase. Since those sites are distributed over the city area and are not related to each other (BOHR1 is situated to the North, AVP in the middle and PFS06 to the South), we do not interpret this behaviour.

The match between measured and modelled dispersion curves is shown in Figs. 7-9 and the match between measured H/V ratio and modelled Rayleigh wave ellipticity is displayed in Fig. 10.

Black lines and error bars indicate the measured dispersion curves, the coloured lines show dispersion curves back calculated from the shear wave profiles resulting from the inversion. Since the misfit ranges are different, we cannot show one colourbar fitting all figures and due to lack of space, we cannot display all colourbars. Labelled colourbars for all arrays can be found in Fig.11.

Half of the fundamental dispersion curves spans a frequency range from approximately 0.5 Hz to 15 or 25 Hz. The other half stops at frequencies of 2-7 Hz, when a higher mode dispersion curve branch takes over. The lowest frequencies were reached for array BOHR1 (0.35 Hz). For most of the fundamental mode dispersion curves (Fig. 7), the overall shape of the curve could be fitted well. The largest discrepancies between measured and modelled curves can be seen at low frequencies reflecting the properties of the deeper underground (see e.g. BOHR1, BOHR2 and WIEBEL). The most unsatisfactory match is found at array KLGV308, lying very near to the rim of the salt diapir.

The higher mode dispersion curves (Fig. 8 and 9) were not easy to fit. The observations span frequency ranges of approximately 3-25 Hz. Interpreting the higher mode observations as first higher mode, the most satisfactory fit was reached for array SPRUETZ, and it is most unsatisfactory for arrays CRAN, JEN2 and NIE (Fig. 8). The interpretation of dispersion curve branches as second higher modes (Fig. 9) show a good fit for site JEN1. For BOHR1, the gradient of the dispersion curve can be fitted well, whereas the average slowness is too low.

Fig. 10 shows the match between measured H/V ratio and Rayleigh wave ellipticity back calculated from the shear wave velocity profile resulting from the last model run of the dispersion curve inversion. H/V ratio and Rayleigh wave ellipticity cannot be equated in general, but show similar peak values if the impedance contrast in the subsurface is high (Malischewsky and Scherbaum, 2004). Although only the H/V peak frequency and not the shape of the ellipticity curve was used in the inversion, the overall shape of ellipticity curves, in particular the width of the frequency peak, fits well. In most cases, the depth of the trough following the peak is overestimated. The increase in amplitude towards the low-frequency limit of the curves is most likely due to tilt of the instruments, caused by e.g. moving vehicles nearby or buildings loaded by wind (Forbriger, 2007).

The array measurements can only give localised information on the diapir. Fig. 11 compares the results from the inversion of dispersion curves to the caprock interface depth extracted from the H/V measurements. On the margin, S-wave velocity profiles derived from dispersion curve inversion are shown. The corresponding P-wave velocities are not as restricted as the S-wave velocities by the inversion and are therefore only displayed in the appendix. This is not surprising, since the phase velocity of Rayleigh waves is ten times more sensitive to the S-wave structure than it is to the P-wave structure (Okada and Sakajiri, 1983).

Each profile indicates a whole range of possible subsurface models which are discriminated by their colour corresponding to the misfit value (see respective colourbars). Velocities beneath the impedance contrast are only resolved poorly which is caused by the sedimentary cover acting as high pass filter and thus limiting the analysable frequency band towards the lower frequencies (Cornou et al, 2006). Therefore, no discrimination can be made between caprock (gypsum, anhydrite) and actual salt diapir.

Arrays are identified by their name and arrows point to their location on the map. On the map, the depth of the main impedance contrast is denoted by a coloured circle using the same colour scale as the H/V-derived pseudo depth in the background. The interface depth resulting from array BOHR2 cannot be displayed since it is located too deep and therefore outside the colour range. Since the position for this array was chosen deliberately within the region where the salt diapir is known to almost reach the surface, the most likely explanation is that either the simple layer-over-halfspace model chosen for dispersion curve inversion is not valid for this site and thus, the real interface depth could not be resolved, or the layering is not horizontal as assumed for the dispersion curve inversion (see Section 4.1). In any case, the interface depth of approximately 1600 m as suggested by dispersion curve inversion is well below the maximum resolvable depth for this array (estimated to be 860 m as one third of the wavelength computed from lowest frequency and slowness values of the dispersion curve) and thus cannot be interpreted. In most cases, the interface depths derived from array measurements agree with the caprock depth obtained from H/V peak frequencies. For arrays AVP and PFS06, situated between the western and eastern high of the diapir in the South of the city area, as well as array KLGV308 at the eastern rim of the salt diapir, the shear wave velocity profiles indicate a larger depth of the interface than the H/V measurements.

4 Discussion

4.1 1-D, 2-D or 3-D?

The inversion of dispersion curves is performed assuming that layering in the subsurface is horizontal. We analysed this assumption treating the array stations as single stations

and computing their H/V peak frequencies. The heterogeneity of the H/V frequency peaks is demonstrated in Fig. 12. The figure in the middle displays the gridded H/V-derived pseudo depth. Points indicate the variability of H/V values across an array using a colour scheme from green (little variability) to red (high variability). The variability has been computed as difference between largest and lowest H/V value within the same array. The size of the points corresponds to the size of the array, since variations in interface depth are more likely to occur beneath a larger array. Figures at the rim show the difference of the single station's H/V peak frequency from the mean H/V peak value across this array, the values being normed over the H/V peak frequency values from all arrays (see colour scale in blue-to-red). A positive value means that the H/V peak frequency at this station is higher than the average value within this array and corresponds to a more shallow impedance contrast. Surprisingly, the largest deviations of H/V peak values across an array do not occur within the largest arrays, but within the arrays in the South being situated above the shallowest updoming of the diapir. It is largest for array BOHR2, being visible as black point, since the variation of peak frequencies across the array is so large that it cannot be imaged using the same colour scale as for the other arrays (instead, a different colour scale is given beneath the sketch of array stations). The second largest differences occur within arrays CRAN and PFS06. Also arrays DIEB, AVP and NIE (the last-mentioned is situated above a salt diapir high near its rim) show a larger variability of H/V frequencies. At the same time, for arrays AVP, BOHR2 and PFS06, the interface depths gained from dispersion curve inversion does not coincide with the H/V pseudo depth. The misfit is especially large for array BOHR2. We think that this indicates either that the gypsum interface has a strong topography or that the interface itself is not smooth, but rather rugged, which could be an indicator of dissolution processes at the gypsum-ground water contact. Both possible explanations violate the assumption on horizontal layering in the subsurface.

There are several studies analysing results of the H/V method in areas where subsurface layers are subjected to strong topography. One bundle of studies deals with resonance effects resulting from basin topography, e.g. in the Tamar valley, Tasmania (Claprood and Asten, 2008) or in the Grenoble valley (Cornou et al, 2003; Guéguen et al, 2007). They state that the largest difference between theoretical evaluations of the 1-D response of the basin and experimentally derived values stem from locations at the edges of the basin, where the subsurface is most heterogeneous, sediments are thinnest and the bedrock topography is strongest.

A second bundle of studies deals with more step-like topographies. Cara et al (2008) compared frequency peaks and amplification of H/V ratios with subsurface geology to map the presence of soft sediments in Palermo and find less reliable results in zones where the spatial variability of sedi-

ments is high, such as the edges of riverbeds and the transition zones between fluvial and sea deposits. The SESAME group (2005) and Bonnefoy-Claudet et al (2004) state that in simulations of laterally varying subsurface topography, H/V curves show clear peaks above topographically flat parts, whereas H/V peaks are broader and generally lower above sites experiencing rapidly varying thickness. Nevertheless, the bandwidth of the broad peaks is generally indicative of the fundamental frequency variations between the shallowest and deepest sections. They advise to perform measurements above suspected topographic variations in a dense grid.

Especially above the southern part of the salt diapir, the subsurface topography can be locally very steep. Although indicators as broad peaks or multiple peaks are present, their occurrence is not localised and is interrupted by sites showing spectra with clear H/V peaks. We conclude therefore that our measurement grid has been dense enough to allow for a meaningful estimation of the depth of the impedance contrast. The dispersion curves most likely reflect an average thickness and S-wave velocity profile across the array (Bonnefoy-Claudet et al, 2004).

4.2 Interpretation of measurement results

The subsurface of Hamburg is complex, consisting of the salt diapir, a caprock made of gypsum and partly anhydrite, overlaid by sand, sandstone and partly by clay. Depending on the local geology, it may be possible that in different parts of the study area not always the same stratum will cause the dominant H/V peak. The relation converting H/V peak frequency into pseudo depth is developed using the first impedance contrast found in borehole stratigraphies regardless of the nature of the underlying material. However, only boreholes where the layer causing the peak in the frequency spectrum can be identified by modelling are employed for this purpose. The remaining boreholes, often containing both a clay and a gypsum interface, will be used here to analyse which impedance contrast is measured by the H/V method (Fig. 13). The background shows the gridded pseudo depth derived from H/V measurements. On the left, clay interface depths are indicated by circles, whereas on the right, gypsum interface depths are marked by stars. In the South of the diapir, clay and gypsum depths do not differ much, but in the North, it is clearly visible that the H/V-derived pseudo depth fit the gypsum interface much better than the clay interface. Together with the relative low contrast between sediment and clay shear wave velocities, we therefore conclude that the impedance contrast measured by the H/V method corresponds to the sediment-gypsum interface.

At the same time as the ambient noise measurements, a gravimetry survey over the same city area has been performed and a 3-D salt topography model has been constructed by Dahm et al (2010b). Fig. 14 compares the results from all three types of measurements: gravity, H/V and array. The

comparison between H/V- and gravity-derived pseudo depths is shown on the left, between H/V- and array-derived pseudo depths in the middle and between gravity- and array-derived pseudo depths on the right. On the left and in the middle, the background shows the gridded pseudo depth derived from the H/V measurements. Since the comparison between H/V and array measurements has already been displayed before (Fig. 11), we use this figure to indicate the array names. On the left, points in the foreground indicate pseudo depths obtained from the inversion of gravity data (Dahm et al, 2010b). A gridded version of these pseudo depths can be found on the right. In the middle and on the right, points in the foreground display pseudo depths obtained from the inversion of dispersion curves.

The overall trend in pseudo depths is the same. However, there are several regions where the gravity-derived pseudo depth differs considerably from the H/V-derived pseudo depth:

- The gravity-derived diapir interface shows a much larger depth at the northern and southern rim of the salt diapir.
- The south-east situated depression seen in the H/V pseudo depth is not contained in the gravity-derived pseudo depths and should be regarded as doubtful since its presence is only based on a single measurement.
- The gravity-derived pseudo depths show a depression in the middle of the diapir in its northern part. The western rim is more distinct in the gravity-derived pseudo depths (very striking south of 53°36'), whereas the eastern rim is more distinct in the H/V pseudo depth.
- The shallow part of the diapir in the South is divided into a eastern and a western part in the gravity-derived pseudo depths, but appears not as separated in the H/V pseudo depth.

As the subsurface topography modelled by gravity and the results estimated from ambient noise measurements show considerable differences, we hypothesize that the stratigraphic boundary related to these subsurface images is not necessarily the same.

The deviation between results from H/V and array measurements has already been described in Section 3.3. The depression in the mid-northern part of the diapir seen by gravity measurements does not agree with the array measurements either. Array KGLV308 suggests a deeper position of the interface which agrees with the location of the Quaternary channel Ellerbeker Rinne as displayed in Fig. 6 in agreement with the H/V-derived pseudo depth. Whereas for arrays AVP and PFS06, situated between the western and eastern high of the diapir in the South of the city area, the shear wave velocity profiles indicate a larger depth of the interface than the H/V measurements, being thus more in agreement with the gravity measurements, arrays JEN1 and JEN2 clearly agree more with the H/V-derived pseudo depth. On the other hand, the variability of H/V peak frequencies is very large for array PFS06 and recognisable for

array AVP violating the horizontal layering assumption for the inversion of dispersion curves (Section 4.1), such that we do not want to attach too much importance to their resulting shear wave profiles. Therefore, we conclude that H/V and array measurements agree in general and most likely see the same interface. Nevertheless, results may disagree to a certain extent since from H/V measurements, only one value per site is extracted, representing a much larger non-uniqueness in interpretation, whereas an array measurement results in a complete dispersion curve, containing much more information.

Gabriel et al (2003) point out that porosity is an important parameter that very much affects physical properties such as density and seismic velocities and that therefore, the seismic impedance is very sensitive to porosity changes. Especially the unconsolidated deposits of the North German lowlands reveal a large variation in petrographic compositions and grain-size distributions, leading to a large variation in physical properties. A very tentative interpretation of the differences between gravity- and ambient noise-derived pseudo depth is that in the South of the OLD, the gypsum layer has probably weathered already, since it is situated at very shallow depths. This weathering may have affected the density of the gypsum much more than its seismic velocity. Thus, its density may not be too different from the density of the overlying sandstone and it may not be recognised by gravimetry measurements. Gravimetry measurements are instead sensitive to deeper layers, consisting e.g. of more compacted gypsum, an anhydrite-gypsum composite or rock salt, having a much higher density. At the same time, the difference in seismic velocities for sandstone and the weathered gypsum layer is large enough to be identified by the H/V measurements. The gypsum layer in the North may not be as weathered, lying deeper, or it may be much thinner or even absent, thus H/V and gravity measurements agree better. This would mean that the H/V method would be a much better indicator of residual caprock and hence karst systems.

5 Conclusions

High quality ambient noise array measurements have been performed efficiently in a logistically and measurement-technology demanding environment (city area) thanks to a recently developed wireless array analysis system. Resulting Rayleigh wave dispersion curves could be used up to a frequency range of 15 - 20 Hz, a frequency range hitherto reserved for MASW techniques (Multichannel Analysis of Surface Waves, see e.g. Park et al, 1999). Numerous H/V measurements allow for a detailed construction of the 3-D gypsum caprock interface of the salt diapir, providing a base for a hazard assessment of regions vulnerable to or already affected by karst. A comparison to gravimetry measurements shows that the H/V method may be a much better indicator of residual caprock and hence karst systems, since it seems

more sensitive to the detection of already weathered gypsum layers.

Acknowledgements The project HADU was granted by the Federal Ministry of Education and Research within the program GEOTECHNOLOGIEN. The State Ministry for Urban Development and the Environment, the Geological Survey of Hamburg (especially J. Kröger), the State Environmental Agency of Schleswig-Holstein (especially R. Kirsch) as well as the Leibniz Institute for Applied Geosciences (especially H. Wiederhold) generously provided data of different kinds. Special thanks to H. Beyer, J. Lücke, M. Ruhnau and C. Sperling without whom such numerous measurements could not have been acquired. In addition, we would like to thank our reviewers U. Wegler and F. Krüger whose comments greatly improved our manuscript. Figures, if not output of software package *geopsy*, were produced using GMT (Wessel and Smith, 1991).

References

Aki K (1957) Space and time spectra of stationary stochastic waves with special reference to microtremors. Bull Earthqu Res Inst 35:415–456

Arai H, Tokimatsu K (1998) Evaluation of local site effects based on microtremor H/V spectra. In: Kudo K, Okada H, Sasatani T (eds) Proc 2nd Int Symp on Effects of Surface Geology on Seismic Motion, Yokohama, Japan, Balkema, vol 2, pp 637–680

Arai H, Tokimatsu K (2004) S-wave velocity profiling by inversion of microtremor H/V spectrum. Bull Seism Soc Am 94(1):53–63

Asten M, Henstridge J (1984) Array estimators and the use of microseisms for reconnaissance of sedimentary basins. Geophys 49(11):1828–1837

Baldschuh R, Fritsch U, Kockel F (2001) The basement block pattern in Northwest Germany. In: Baldschuh R, Binot F, Fleig S, Kockel F (eds) Geotektonischer Atlas von Nordwest-Deutschland und dem deutschen Nordsee-Sektor, Schweitzerbart

Bard PY (1999) Microtremor measurements: a tool for site effect estimation? In: Kudo K, Okada H, Sasatani T (eds) Proc 2nd Int Symp on the Effects of Surface Geology on Seismic Motion, Yokohama, Japan, Balkema, vol 3, pp 1251–1279

Benito G, del Campo P, Gutierrez-Elorza M, Sancho C (1995) Natural and human-induced sinkholes in gypsum terrain and associated environmental problems in NE Spain. Environ Geol 25:156–164

Birgören G, Özel O, Siyahi B (2009) Bedrock depth mapping of the coast south of Istanbul: comparison of analytical and experimental analyses. Turkish J Earth Sci 18:1–15

Bonnefoy-Claudet S, Cornou C, Kristek J, Ohrnberger M, Wathelet M, Bard PY, Moczo P, Fäh D, Cotton F (2004) Simulation of seismic ambient noise: I. Results of H/V and array techniques on canonical models. In: XIII WCEE, Vancouver, Canada, August 1-6, 2004, Paper No. 1120

Buurman N (2009) Charakterisierung von Zirkularstrukturen im geologischen Untergrund Hamburgs zur Abgrenzung verkarstungsgefährdeter Bereiche. PhD thesis, University of Hamburg, Germany, 279pp

Capon J (1969) High-resolution frequency-wavenumber spectrum analysis. In: Proc IEEE, vol 57, pp 1408–1419

Cara F, Cultrera G, Azzara RM, De Rubeis V, Di Giulio G, Giammarinaro MS, Tosi P, Vallone P, Rovelli A (2008) Microtremor measurements in the city of Palermo, Italy: analysis of the correlation between local geology and damage. Bull Seism Soc Am 98(3):1354–1372

Claprood M, Asten MW (2008) Microtremor survey methods in the Tamar Valley, Launceston, Tasmania: evidence of 2D resonance from microtremor observations. In: Proc Earthquake Eng, Australia Conference 2008, Austr Earthqu Eng Soc

Cornou C, Bard PY, Dietrich M (2003) Contribution of dense array analysis to the identification and quantification of basin-edge induced waves. Part II: Application to Grenoble basin (French Alps). Bull Seism Soc Am 93(6):2624–2648

Cornou C, Ohrnberger M, Boore DM, Kudo K, Bard PY (2006) Derivation of structural models from ambient vibration array recordings: results from an international blind test. In: Proc 3rd Int Symp on the Effects of Surface Geology on Seismic Motion, Grenoble, France, 30 August - 1 September 2006

Dahm T, Heimann S, Biawolons W (2010a) A seismological study of shallow week earthquakes in the urban area of Hamburg city, Germany, and its possible relation to salt dissolution. Nat Haz Submitted

Dahm T, Kühn D, Ohrnberger M, Kröger J, Wiederhold H, Reuther CD, Dehghani A, Scherbaum F (2010b) Combining geophysical data sets to study the dynamics of shallow evaporites in urban environments: application to Hamburg, Germany. Geophys J Int 181(1):154–172

Delgado J, López CC, Giner J, Estévez A, Cuenca A, Mouna S (2000) Microtremors as geophysical exploration tool: applications and limitations. Pure Appl Geophys 157:1445–1462

Ehlers J (1995) Geologische Karte von Hamburg, 1:25000, Erläuterungen zu Blatt Nr. 2425 Hamburg. Tech. rep., Geol. Landesamt Hamburg

Fäh D, Kind F, Giardini D (2001) A theoretical investigation of average H/V ratios. Geophys J Int 145:535–549

Fäh D, Kind F, Giardini D (2003) Inversion of local S-wave velocity structures from average H/V ratios, and their use for the estimation of site effects. J Seismol 7(4):449–467

Fleischhauer CO (1979) Höhenveränderungen im Hamburger Haupt- und Landeshöhennetz. Mitteilungsblatt Vermessungsamt Hamburg 68(1):15–32

Forbriger T (2007) Low-frequency limit for H/V studies due to tilt. In: 67th Annual Meeting DGG, Aachen, Germany

Gabriel G, Kirsch R, Siemon B, Wiederhold H (2003) Geophysical investigation of buried Pleistocene subglacial valleys in Northern Germany. J Appl Geophys 53:159–180

Geluk M, Paar W, Fokker P (2007) Salt. In: Wong T, Batjes D, deJaeger D (eds) Geology of the Netherlands, Royal Academy of Arts and Science, pp 283–294

Gripp K (1920) Steigt das Salz zu Lüneburg, Langenfelde und Segeberg episodisch oder kontinuierlich? Abhandlung zu Vortrag auf Hauptversammlung der Deutschen Geophysikalischen Gesellschaft in Hannover

Grube F (1973) Ingenieurgeologische Erkundung der Erdfälle im Bereich des Salzstocks Othmarschen-Langenfelde (Hamburg). Tech. rep., Geol. Landesamt Hamburg

Guéguen P, Cornou C, Garambois S, Bantou J (2007) On the limitation of the H/V spectral ratio using seismic noise as an exploration tool: application to the Grenoble Valley (France), a small apex ratio basin. Pure Appl Geophys 164:115–134

Hanka W, Heinloo A, Jäckel KH (2000) Networked seismographs: GEOFON real-time data distribution. Orfeus Newsletter 2(3): http://www.orfeus-eu.org/newesletter/newsletter.htm

Hinzen KG, Scherbaum F, Weber B (2003) On the resolution of H/V measurements to determine sediment thickness, a case study across a normal fault in the Lower Rhine Embayment, Germany. J Earthquake Eng 8(6):906–926

Horike M (1985) Inversion of phase velocity of long-period microtremors to the S-wave velocity structure down to the basement in urbanized areas. J Phys Earth 33:59–96

Ibs von Seht M, Wohlenberg R (1999) Microtremor measurements used to map thickness of soft soil sediments. Bull Seismol Soc Am 89:250–259

Ishida H, Nozawa T, Niwa M (1998) Estimation of deep surface structure based on phase velocities and spectral ratios of long-period microtremors. In: Kudo K, Okada H, Sasatani T (eds) Proc 2nd Int Symp on Effects of Surface Geology on Seismic Motion, Yokohama, Japan, Balkema, vol 2, pp 697–704

Jaritz W (1987) The origin and development of salt structures in NW Germany. In: Lerche I, O'Brien J (eds) Dynamical Geology of Salt and Related Structure, Academic Press, Orlando, pp 479–493

Johnson KS (2008) Gypsum-karst problems in constructing dams in the USA. Environ Geol 53:945–950

Jongmans D, Ohrnberger M, Wathelet M (2005) Recommendations for array measurements and processing. Deliverable D24.13, available at http://sesame-fp5.obs.ujf-grenoble.fr/Delivrables/Del-D24-Wp13.pdf

Kawase H, Satoh T, Iwata T, Irikura K (1998) S-wave velocity structures in the San Fernando and Santa Monica areas. In: Kudo K, Okada H, Sasatani T (eds) Proc 2nd Int Symp on Effects of Surface Geology on Seismic Mo-

tion, Yokohama, Japan, Balkema, vol 2, pp 733–740

Konno K, Ohmachi T (1998) Ground-motion characteristics estimated from spectral ratio between horizontal and vertical components of microtremor. Bull Seism Soc Am 88(1):228–241

Lachet C, Bard PY (1994) Numerical and theoretical investigations on the possibilities and limitations of Nakamura's technique. J Phys Earth 42:377–397

Malischewsky P, Scherbaum F (2004) Love's formula and H/V ratio (ellipticity) of Rayleigh waves. Wave Motion 40(1):57–67

Matsushima T, Okada H (1990) Determination of deep geological structures under urban areas. J Soc Explor Geophys Jpn 34:21–33

Michel C, Guéguen P, Bard PY (2008) Dynamic parameters of structures extracted from ambient vibration measurements: an aid for the seismic vulnerability assessment of existing buildings in moderate seismic hazard regions. Soil Dyn Earthqu Eng 28:593–604

Miyakoshi K, Kagawe T, Kinoshita S (1998) Estimation of geological structures under the Kobe area using the array recordings of microtremors. In: Kudo K, Okada H, Sasatani T (eds) Proc 2nd Int Symp on Effects of Surface Geology on Seismic Motion, Yokohama, Japan, Balkema, vol 2, pp 691–696

Mooney HM, Bolt BA (1966) Dispersive characteristics of the first three Rayleigh modes for a single surface layer. Bull Seism Soc Am 56(1):43–67

Nakamura Y (1989) A method for dynamic characteristics estimation of subsurface using microtremor on the ground surface. QR RTRI 30:25–33

Niedermayer J (1962) Die geologischen Verhältnisse im Bereich des Salzstocks von Hamburg-Langenfelde. Mitteilung Geol Landesamt Hamburg 39:167–175

Nogoshi M, Igarashi T (1971) On the amplitude characteristics of microtremor (part 2). J Seism Soc Japan 24:26–40, (in Japanese with English abstract)

Ohrnberger M, Schissele E, Cornou C, Bonnefoy-Claudet S, Wathelet M, Savvaidis A, Scherbaum F, Jongmans D (2004a) Frequency wavenumber and spatial autocorrelation methods for dispersion curve determination from ambient vibration recordings. In: XIII WCEE, Vancouver, Canada, August 1-6, 2004, Paper No. 0946

Ohrnberger M, Schissele E, Cornou C, Wathelet M, Savvaidis A, Scherbaum F, Jongmans D, Kind F (2004b) Microtremor array measurements for site effect investigations: comparison of analysis methods for field data cross-checked by simulated wavefields. In: XIII WCEE, Vancouver, Canada, August 1-6, 2004, Paper No. 0940

Ohrnberger M, Schissele E, Cornou C, Wathelet M, Bonnefoy-Claudet S, Savvaidis A, Di Giuglio G, Guillier B, Köhler A, Roten D, Scherbaum F, Jongmans D, Vollmer D (2005) Report on the FK/SPAC capabilities and limitations. Deliverable D19.06, available

at http://sesame-fp5.obs.ujf-grenoble.fr/Delivrables/Del-D19-Wp06.pdf

Okada H (2003) The microseismic survey method. Society of Exploration Geophysicists of Japan, translated by Koya Suto, Geophysical Monograph Series No. 12, Society of Exploration Geophysicists

Okada H, Sakajiri N (1983) Estimation of an S wave velocity distribution using long-period microtremors. Geophys Bull Hokkaido Univ 42:119–143, (in Japanese with English abstract)

Paluska A (2002) Geologische Stellungnahme zum Bebauungs-Planentwurf Gross Flottbek 10 (Osdorfer Marktplatz). Tech. rep., Geol. Landesamt Hamburg

Panou AA, Theodulidis NP, Hatzidimitriou PM, Savvaidis AS, Papazachos CB (2005) Reliability of ambient noise horizontal-to-vertical spectral ratio in urban environments: the case of Thessaloniki city (Northern Greece). Pure Appl Geophys 162:891–912

Park CB, Miller RD, Xia J (1999) Multichannel analysis of surface waves (MASW). Geophys 64:800–808

Parolai S, Bormann P, Milkereit C (2002) New relationships between vs, thickness of sediments, and resonance frequency calculated by the H/V ratio of seismic noise for Cologne area (Germany). Bull Seism Soc Am 92:2521–2527

Parolai S, Picozzi M, Richwalski SM, Milkereit C (2005) Joint inversion of phase velocity dispersion and H/V ratio curves from seismic noise recordings using a genetic algorithm, considering higher modes. Geophys Res Lett 32, doi:10.1029/2004GL021115

Picozzi M, Parolai S, Richwalski SM (2005) Joint inversion of H/V ratios and dispersion curves from seismic noise: Estimating the S-wave velocity of bedrock. Geophys Res Lett 32, doi:10.1029/2005GL022878

Picozzi M, Strollo A, Parolai S, Durukal E, Öyel O, Karabulut S, Zschau J, Erdik M (2009) Site characterization by seismic noise in Istanbul, Turkey. Soil Dyn Earthqu Eng 29:469–482

Plaumann S (1979) Schweremessungen über dem Bereich des Salzstockes Othmarschen Langenfelde in Hamburg. Tech. rep., Niedersächsisches Landesamt für Bodenforschung (NlfB)

Prexl A (1997) Geologie von Salzstockdächern. Master's thesis, University of Hannover, Institute of Geology and Paleontology

Reinhold K, Krull P, Kockel F (2008) Salzstrukturen Norddeutschlands: geologische Karte 1:50000. Bundesanstalt für Geowissenschaften und Rohstoffe Hannover

Rumpel HM, Grelle T, Hölscher F, Stoll M (2005) Vertikales seismisches Profil (VSP) zur teufenabängigen Geschwindigkeitsbestimmung im BurVal Meßgebiet Ellerbeker Rinne. Project report

Sambridge M (1999a) Geophysical inversion with a neighbourhood algorithm - I. Searching a parameter space.

Geophys J Int 138:479–494

Sambridge M (1999b) Geophysical inversion with a neighbourhood algorithm - II. Appraising the ensemble. Geophys J Int 138:727–746

Satoh T, Kawase H, Matsushima S (2001) Estimation of S-wave velocity structure in and around the Sendai basin, Japan, using array records of microtremors. Bull Seism Soc Am 91(2):206–218

Scheck-Wenderoth M, Maystrenko Y, Hübscher C, Hansen M, Mazur S (2008) Dynamics of salt basins. In: Littke R, Bayer U, Gajewski D, Nelskam S (eds) Dynamics of salt basins, pp 309–322

Scherbaum F, Hinzen KG, Ohrnberger M (2003) Determination of shallow shear wave velocity profiles in the Cologne, Germany area using ambient vibrations. Geophys J Int 152:597–612

SESAME group (2005) Guidelines for the implementation of the H/V spectral ratio technique on ambient vibrations measurements, processing and interpretation. Deliverable D23.12, available at http://sesame-fp5.obs.ujf-grenoble.fr/Delivrables/Del-D23-HV_User_Guidelines.pdf

Soriano M, Simon J (1995) Alluvial dolines in the Central Ebro basin, Spain: a spatial and developmental hazard analysis. Geomorph 11:295–309

Soriano M, Simon J (2002) Subsidence rates and urban damages in alluvial dolines of Central Ebro basin (NE Spain). Environ Geol 42:467–484

Tokimatsu K (1997) Geotechnical site characterization using surface waves. In: Ishihara K (ed) Proc IS-Tokyo '95, 1st Int Conf Earthquake Geotech Eng, Tokyo, Japan, 14-16 November 1995, vol 3, Balkema, Rotterdam, pp 1333–1368

Tønnesen A (2004) Implementing and extending the optimized link state routing protocol. Master's thesis, University of Oslo, Department of Informatics

Waltham T, Bell F, Culshaw M (2005) Sinkholes and Subsidence. Springer, Chichester, 382pp

Warren JK (2006) Evaporites - Sediments, Resources and Hydrocarbons. Springer, Berlin, 1035pp

Wathelet M (2005) Array recordings of ambient vibrations: surface wave inversion. PhD thesis, Liège University, Belgium, 177pp

Wathelet M (2008) An improved neighborhood algorithm: parameter conditions and dynamic scaling. Geophys Res Lett 35:L09,301

Wathelet M, Jongmans D, Ohrnberger M (2004) Surface wave inversion using a direct search algorithm and its application to ambient vibrations measurements. Near Surf Geophys 2:211–221

Wessel P, Smith WHF (1991) Free software helps map and display data. EOS Trans AGU 72(41):441

Wiederhold H, Agster G, Gabriel G, Kirsch R, Schenck PF, Scheer W, Voss W (2002) Geophysikalische Erkundung

eiszeitlicher Rinnen im südlichen Schleswig-Holstein. Z Angew Geol 1:13–26

Yamamoto H (1998) An experiment for estimating S-wave velocity structure from phase velocities of Love and Rayleigh waves in microtremors. In: Kudo K, Okada H, Sasatani T (eds) Proc 2nd Int Symp on Effects of Surface Geology on Seismic Motion, Yokohama, Japan, Balkema, vol 2, pp 705–710

Yamanaka H, Takemura M, Ishida H, Niwa M (1994) Characteristics of long-period microtremors and their applicability in exploration of deep sedimentary layers. Bull Seism Soc Am 84:1831–1841

Zimmer U (2001) Quantitative Untersuchung zur Mikrorissigkeit aus akustischen Gesteinseigenschaften am Beispiel von Steinsalz und Anhydrit. PhD thesis, TU Berlin, 191pp

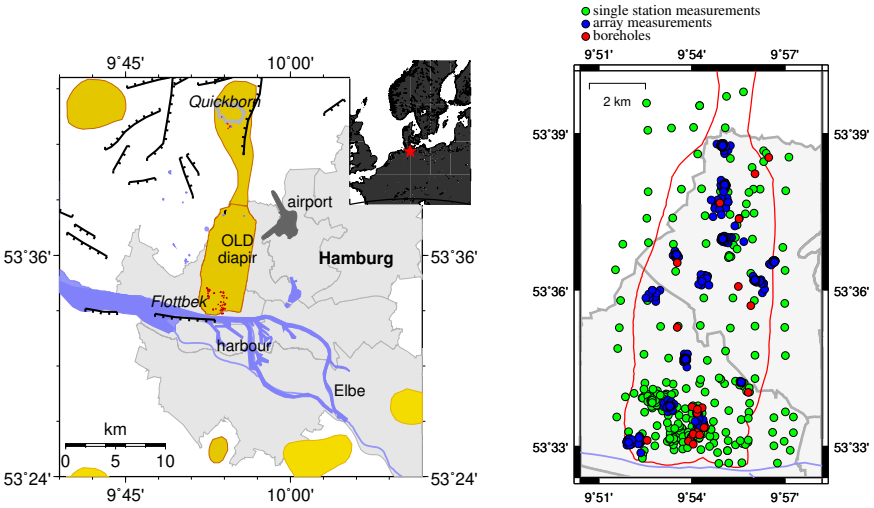

Fig. 1 Left: overview on salt diapirs in Hamburg, Northern Germany (Reinhold et al, 2008), diapirs shown in yellow, Othmarschen-Langenfelde salt diapir (OLD) is indicated; small red polygons on the OLD indicate sinkholes structures (Buurman, 2009); Tertiary Zechstein faults (black lines) are based on reflection seismic profiles and are taken from Baldschuh et al (2001); Hamburg city area and its districts plotted in the background (light grey areas), Quickborn city area indicated by grey circle; right: overview on single station measurements (green points), array measurements (blue points, individual array stations are plotted), and available borehole stratigraphies (red points); OLD outline plotted in red after Grube (1973)

.

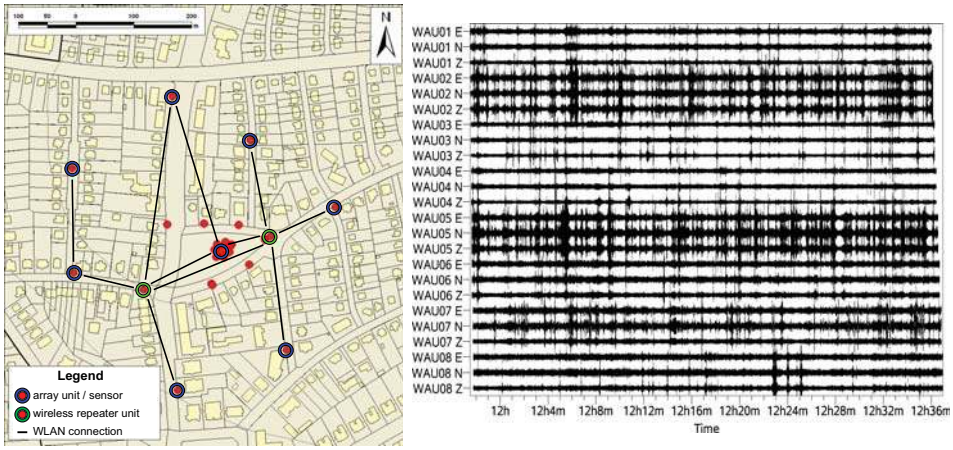

Fig. 2 Left: example of an 8-station array geometry realised in the city area of Hamburg; red circles declare subsequent positions of stations; current configuration is indicated by outward blue circles, while green outward circles indicate repeater nodes, selforganised multipoint-to-multipoint WLAN network indicated by black lines; right: 40 minutes of ambient noise recordings on 8 three-component stations

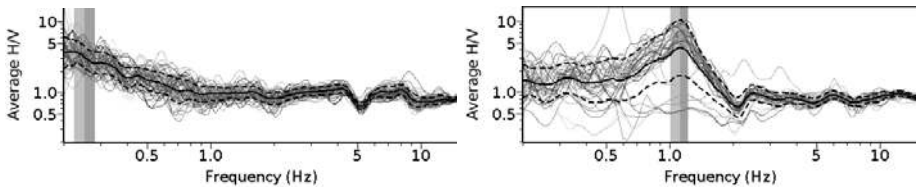

Fig. 3 H/V spectra, grey vertical bars give standard deviation of the automatically identified H/V peak frequency; left: outside salt diapir, right: above salt diapir, H/V peak is clearly visible at 1.1 Hz

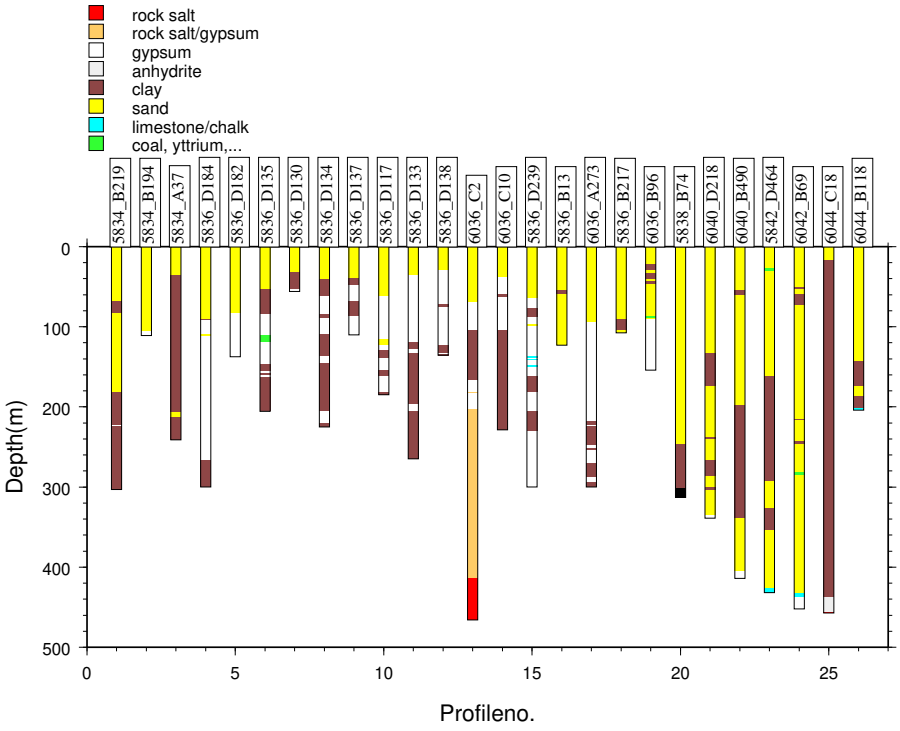

Fig. 4 Borehole profiles sorted by latitude (southernmost to the left, northernmost to the right), labelled; geological layers are identified in legend. The caprock is much more shallow in the South of the city area.

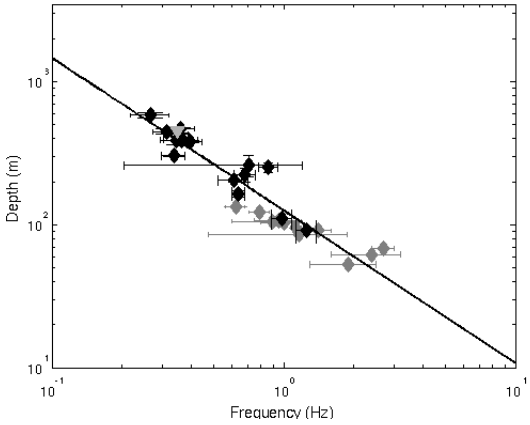

Fig. 5 Regression of frequency-depth data; black diamonds: data derived from dispersion curve inversion, grey diamonds: data derived from H/V measurements at borehole positions, grey triangle: data point resulting from gravity inversion (Dahm et al, 2010b), black line: regression line

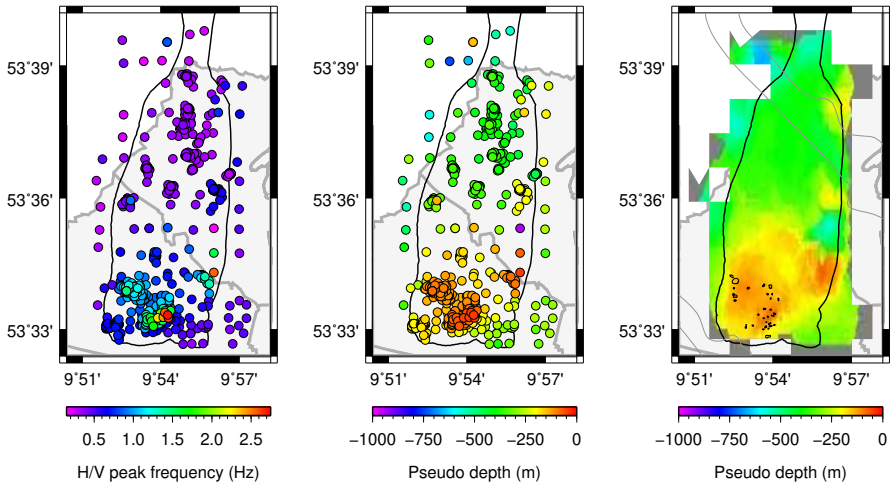

Fig. 6 Left: measured peak frequencies, middle: peak frequencies converted by equation (1) to pseudo depths using a=125.29 and b=-1.07, right: pseudo depth gridded to gain an impression of the interface appearance; thin grey lines to the North mark a Quaternary channel, the Ellerbeker Rinne; polygons to the South (thin black lines) give locations of recent sinkholes

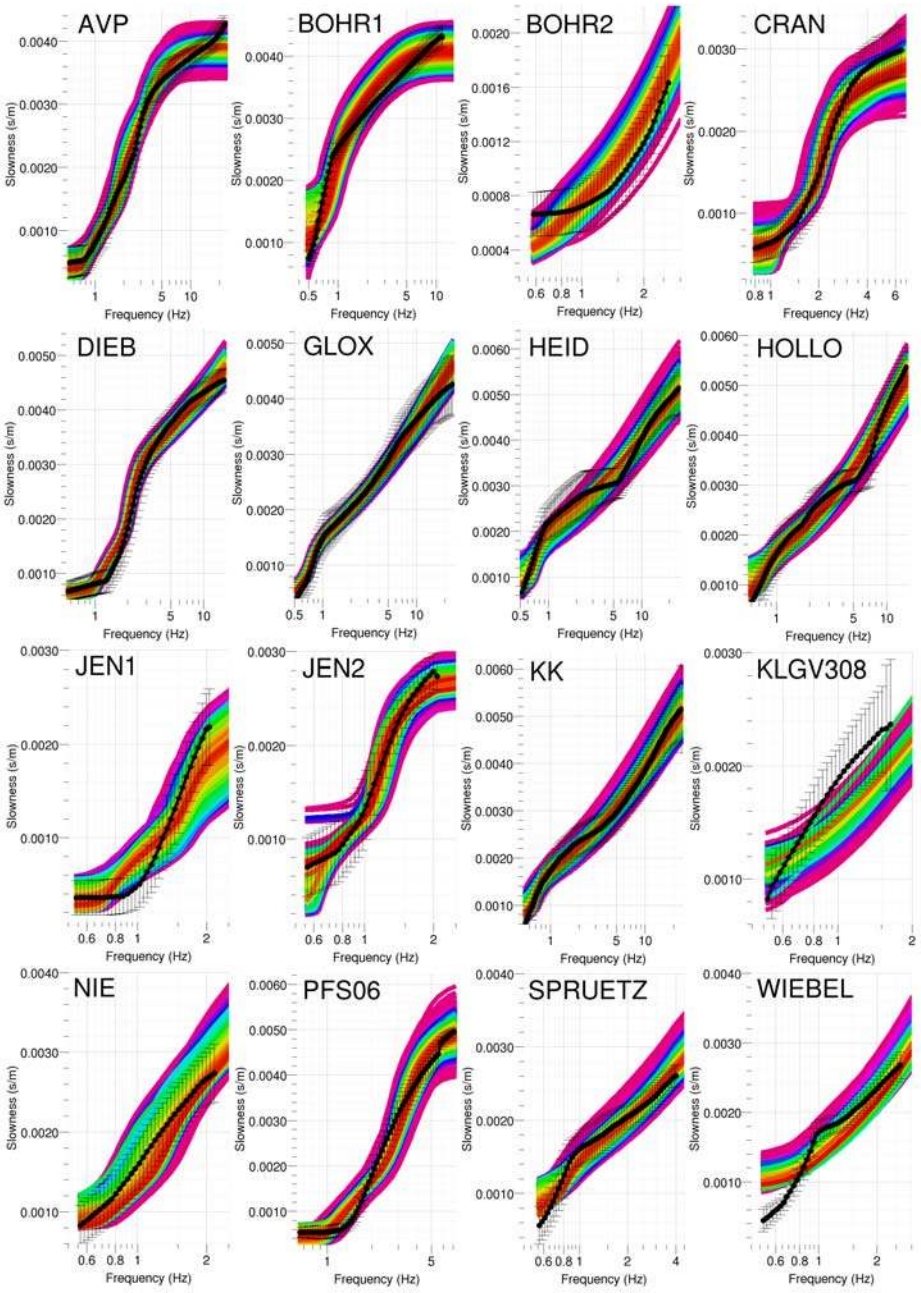

Fig. 7 Fundamental mode dispersion curves; black line and error bars: measured dispersion curve, coloured lines: modelled dispersion curves (for colour bar see Fig. 11); please note that both frequency and slowness axis have different ranges for all figures (scaled to respective minimum and maximum)

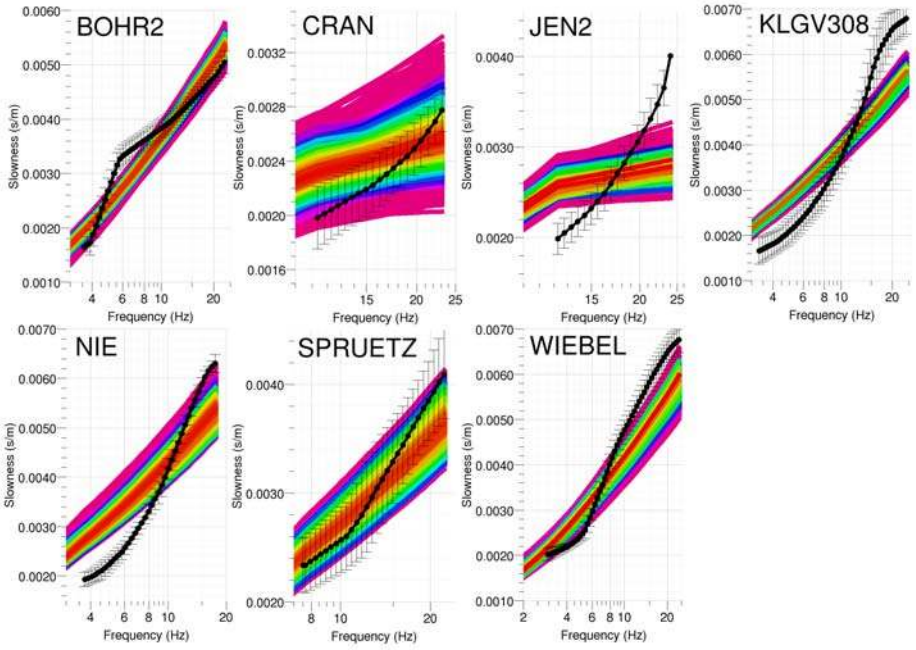

Fig. 8 Higher mode dispersion curve branches interpreted as first higher mode; black line and error bars: measured dispersion curve, coloured lines: modelled dispersion curves (for colour bar see Fig. 11); please note that both frequency and slowness axes have different ranges for all figures (scaled to respective minimum and maximum)

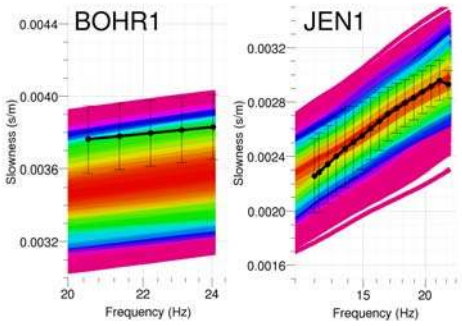

Fig. 9 Higher mode dispersion curve branches interpreted as second higher mode; black line and error bars: measured dispersion curve, coloured lines: modelled dispersion curves (for colour bar see Fig. 11); please note that both frequency and slowness axes have different ranges for both figures (scaled to respective minimum and maximum)

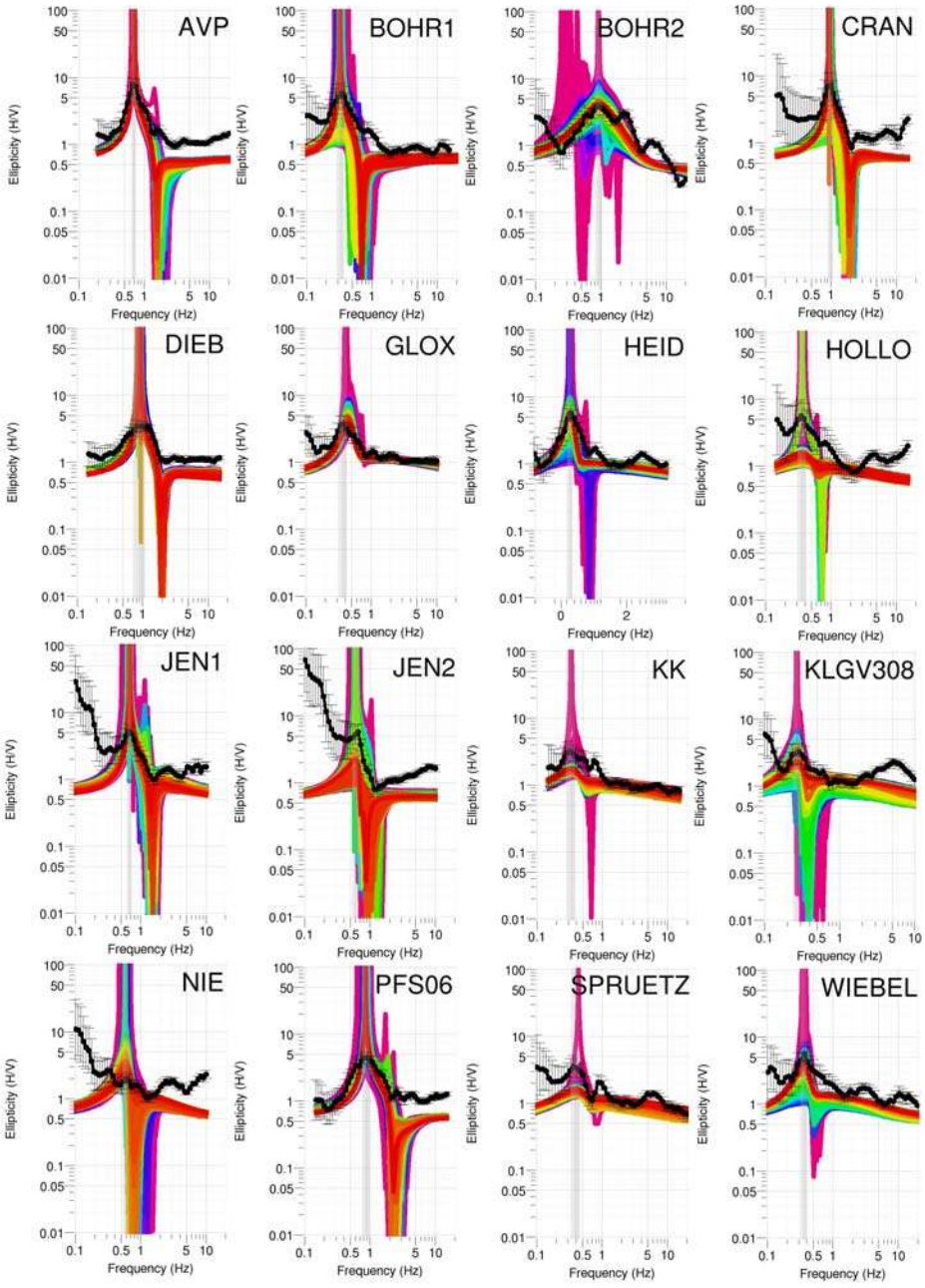

Fig. 10 Comparison between measured H/V ratio (black lines and error bars) and Rayleigh wave ellipticity resulting from last model run (coloured lines)

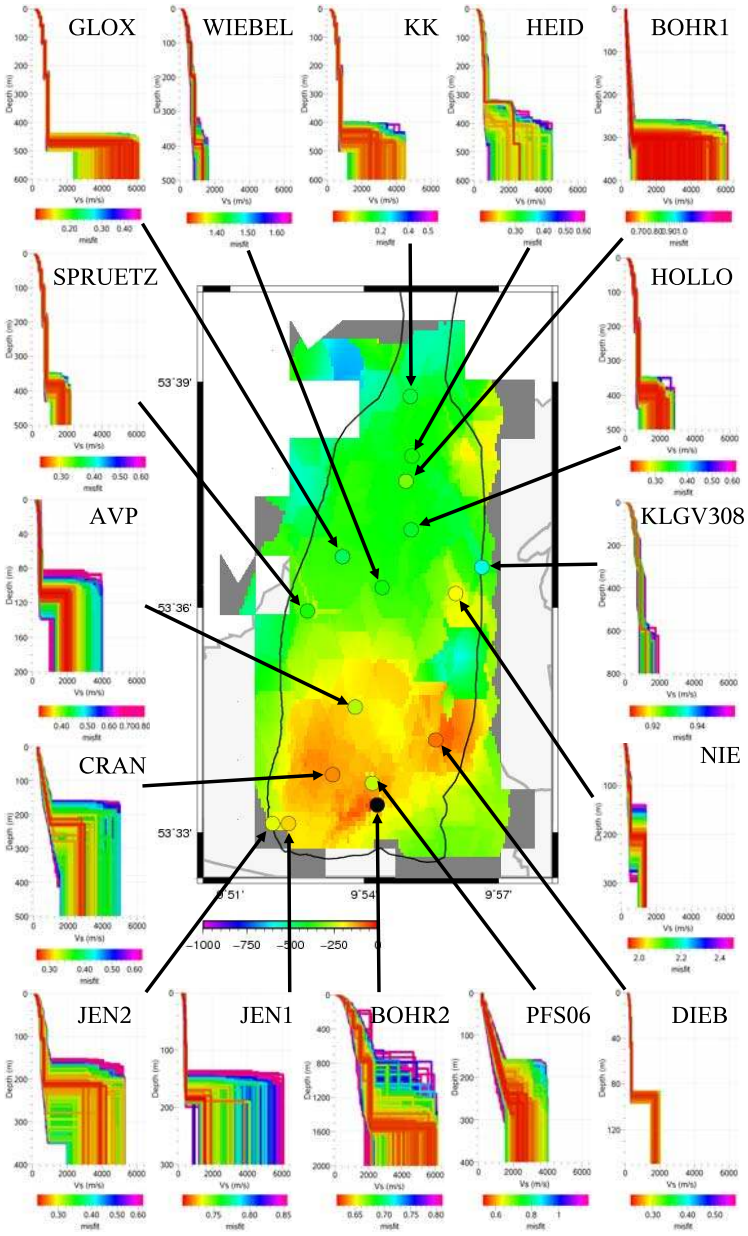

Fig. 11 Middle: background shows gridded pseudo depth, circles give depths of interface derived from dispersion curve inversion; margin: shear wave velocity profiles derived from dispersion curve inversion including misfit colour bars

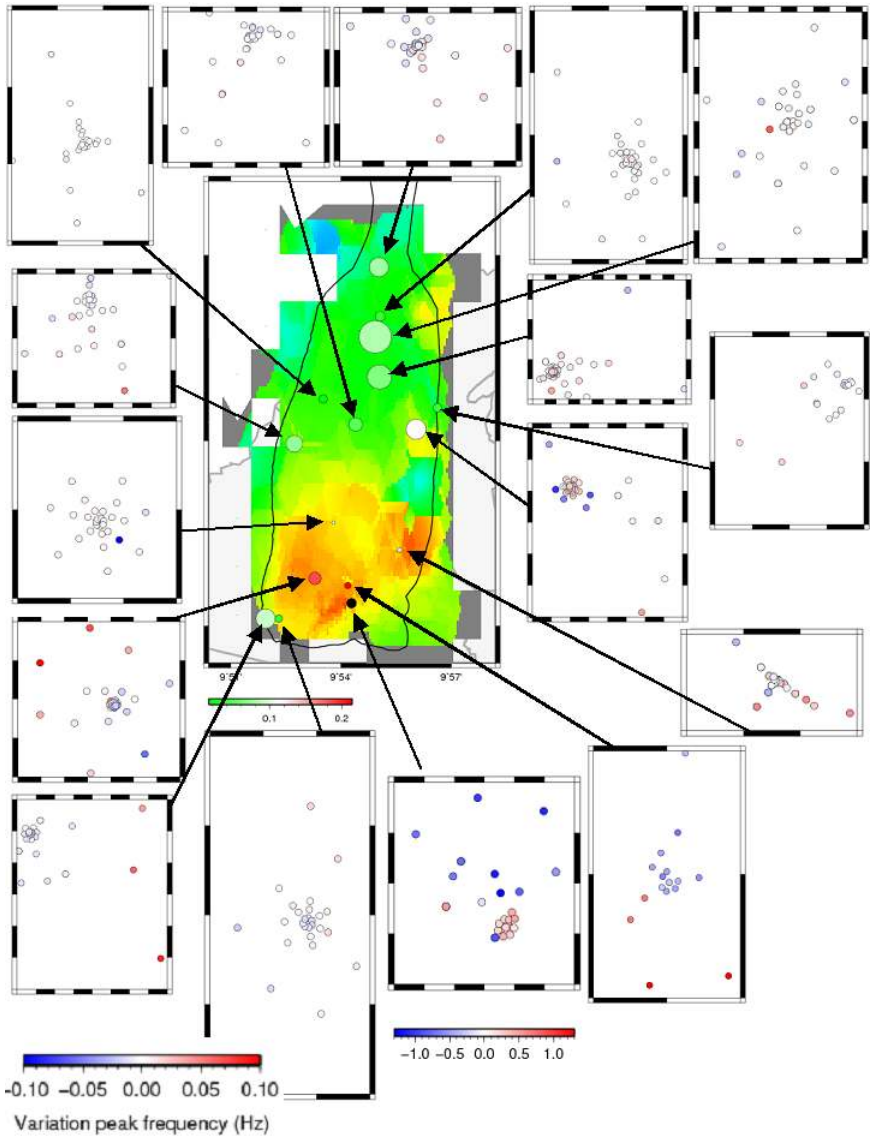

Fig. 12 Heterogeneity of H/V peak frequencies within each array; middle: background: gridded H/V pseudo depth, circles: variability within array colour coded from green (little variability) to red (high variability), circle size indicates array size; surrounding figures: difference between mean H/V peak frequency over array and individual H/V peak frequencies, colour scale from blue (H/V peak frequency lower than mean H/V peak frequency) to red (H/V peak frequency higher than mean H/V peak frequency)

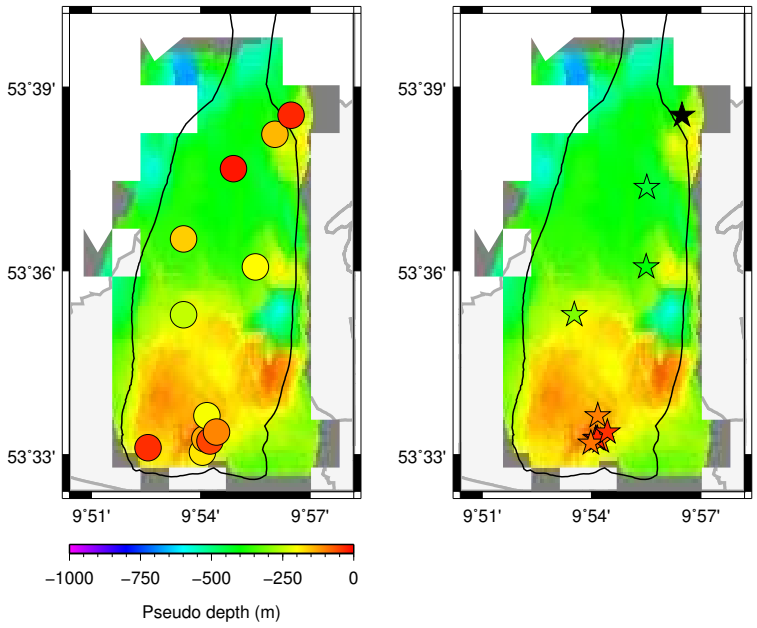

Fig. 13 Comparison between H/V-derived pseudo depth and borehole stratigraphies; background: gridded pseudo depth derived from H/V measurements; left: clay interface depths (circles); right: gypsum interface depths (stars)

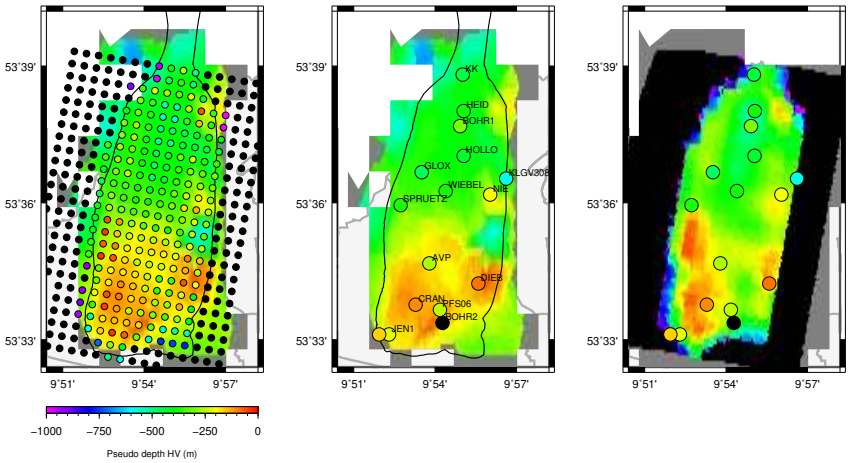

Fig. 14 Comparison between H/V-derived pseudo depth, results from the gravimetric survey by Dahm et al (2010b) and pseudo depths derived from dispersion curve inversion; left: background gives gridded pseudo depth derived from H/V measurements, points indicate pseudo depths obtained from the inversion of gravity data; middle: background gives gridded pseudo depth derived from H/V measurements, points indicate pseudo depths obtained from inversion of dispersion curves; right: background gives gridded pseudo depth derived from gravity measurements, points indicate pseudo depths obtained by inversion of dispersion curves

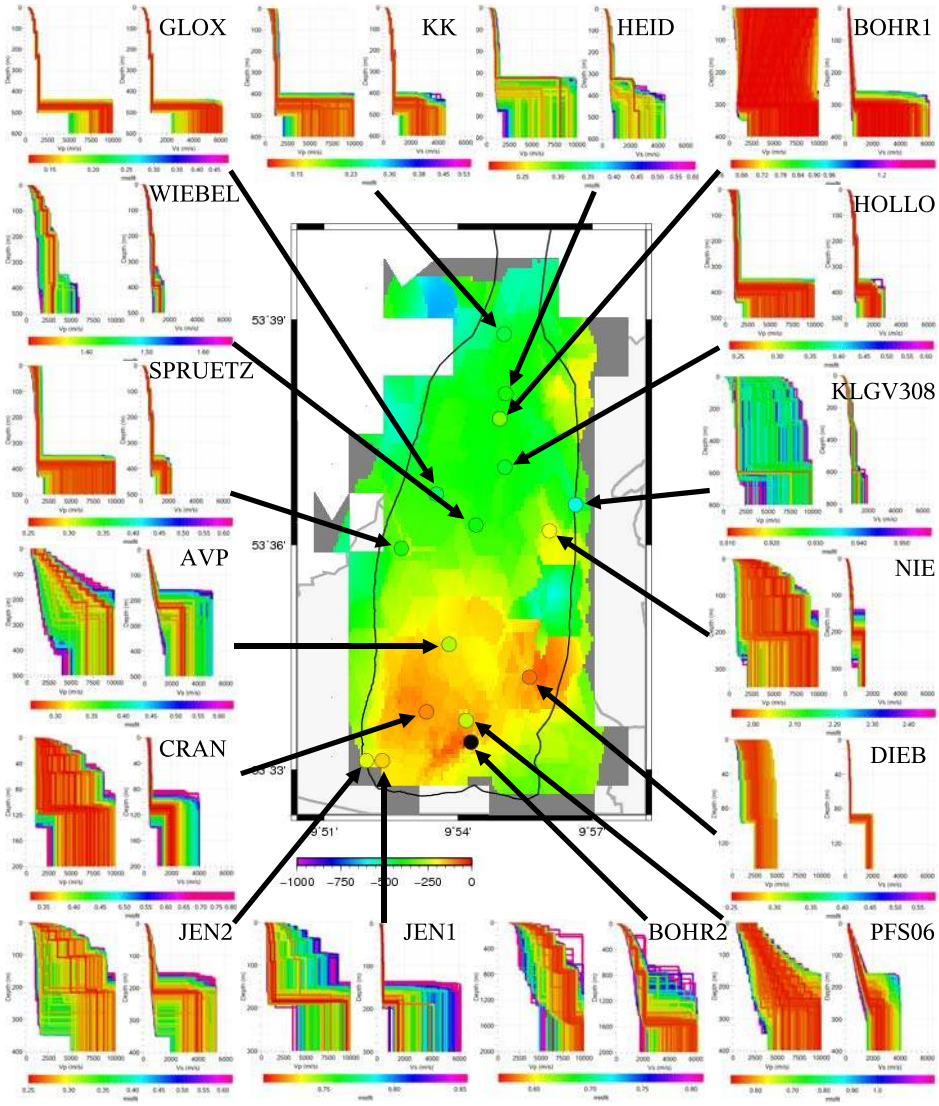

Fig. 15 Middle: background shows gridded pseudo depth derived from H/V measurements, circles give depths of interface derived from dispersion curve inversion; margin: compressional and shear wave velocity profiles derived from dispersion curve inversion including misfit colour bars